ECA, PCA and LaserBall Reconstruction
SNO-STR-00-007

P. Skensved

April 20, 2000

Introduction

This document discusses the Queen's ECA and PCA calibration and shows reconstruction results for laserball runs taken in Feruary 2000 and October 1999. The method is shown to be self consistent and it has been able to identify a number of 'bad' channels (charge and/or time) . As a byproduct it produces single photon electron gains for all active PMTs. It appears (based on the laserball data) to provide a stable PCA calibration within the D_2O volume for average occupancies of less than 30% .

ECA

In this analysis charge pedestals were read from the the standard PECA titles files and used to generate a 'calibrated' charge (Q_{hs}) for each hit phototube. Similarly, the time-slopes were taken from the standard TECA titles files. These were used to convert the raw hit time to an ECA corrected time t_{ECA} with a slightly modified SNOMAN described below.

During a TECA calibration we create pedestal events with different time delays and simply store tables of raw time ADC values as a function of the time delay for each TAC. For real events SNOMAN then does a simple reverse interpolation to convert the raw time ADC value to ECA calibrated time but in the process it makes certain assumptions about the linearity of the TAC. It is a feature of the design that the TACs deviate from a straight line near the end of their ranges (corresponding to early PMT times since the trigger system uses a common stop) . This non-linearity is commonly referred to as TAC curl. Even though the TACs are not linear they are still monotonic and therefore perfectly usable up to the zero slope point. Just to confuse matters, the zero slope point is sometimes also referred to as the TAC curl. As was show at the Sudbury Analysis Meeting there is a feature (bug ?) in the standard SNOMAN code where it flags a tube as invalid if the time is in this intermediate TAC curl region of early time. Approximately one third of all TACs are affected by this to some degree or another. Losing an early PMT will make identification of flasher and PMT β-γ events much more difficult.

The modified Queen's TECA code uses the same interpolation algorithm but does *not* reject the tube unless it is at or beyond the zero slope point. Only PMTs in the extreme TAC curl region are flagged as invalid.

In all of the following we use pedestal corrected Q_{hs} as a measure of the charge. No attempt has been made to correct for the charge gain determined from the charge injection (QECA) runs.

PCA Stage 1

The PCA corrects for such things as differences in cable lengths, discriminator walk, differences in backplane wiring etc. It can in principle be done from an ASYNC triggered laser run at any location in the detector but in practise there are advantages to placing the laserball exactly in the center of the PSUP as will be discussed later. Furthermore, since we are primarily interested in solar neutrino data we restrict ourselves to relatively low intensity runs with occupancy of about 5%. This reduces the chance of being influenced by photons hitting the dynode directly causing large discontinuities in the walk.

Assuming the laserball is at $\vec{r}$ and the position and ECA corrected hit time of the i'th PMT is $\vec{r_i}$ and t_i respectively we can create and histogram the time residuals :

$$\Delta t_i = t_i - \frac{n}{c}|\vec{r_i} - \vec{r}| - T_0 \tag{1}$$

where T_0 is a constant choosen such that Δt_i averaged over all events and all PMTs is zero. T_0 is about 278 ns for the current detector configuration for 500 nm light. It changes with wavelength since the laser trigger is generated at the laser itself but the light has to travel through 100' of fiber. The histogramming is done with a cut on Q_{hs}. The value and the justification for this cut will be discussed later. For the PMT positions we do *not* use the center of the front face of the reflectors from the SNOMAN database but something closer to the 'optical center' of the PMT which is further back. This is a second order effect when the laserball is off center but there is no reason not to correct for it. At present we use the same refractive index for both D_2O and H_2O when calculating the residuals (more on this later) .

Next step is to find the centroid of the prompt peak in the time residual histogram for each active channel. This is done in an iterative way using sliding a narrow time window around the peak starting with the channel with the most count. This gives us the average walk correction for each channel. Figure 1 shows a typical Δt_i histogram and figure 2 shows the corresponding Q_{hs} histogram. The average walk correction $\Delta t_i^{(av)}$ is plotted as a function of detector channel number (starting at crate 0/card 0/channel 0) in figure 3. There is a clear correlation between where a PMT is in channel/card/crate space and what its average walk is. This is presumably due to trigger routing on the backplane since the PMT cables are all the same length to better than 1%. Channels for which the DQCR status word ANDed with 0x207 is non-zero (ie. 'no PMT cable', 'no HV resistor', 'sequencer disabled' or 'not operational') are excluded in this PCA. Also excluded are OWL, BUTT and NECK channels. In addition, PMTs which have no counts in their Q_{hs} histograms are flagged (as '0' occupancy) . In principle LowGain PMTs are not excluded but in practise they all get classified as '0' occupancy.

In addition to determining the average walk for each channel the code also calculates the single photo electron (SPE) gain for each channel. This is done using the algorithm from the original Queen's PMT testing. There we defined the SPE gain as the centroid of the charge spectrum when integrating between 0.25 and 2.5 SPE . It is found by iteration and usually converges in less than 4 passes. Figure 4 shows the SPE gain (in channels above pedestal) as a function of channel number for PMTs with and without blown 75 Ω terminators. The PMT gains are surprisingly uniform across the detector.

The output from this stage (average walk for each channel, lower Q_{hs} cut, Q_{SPE} and tube status/type) is stored in a 'PZERO' titles file which can be read back into SNOMAN and the code will open a ROOT graphical browser which lets the user manipulate individual Q_{hs} or TAC histograms.

PCA Stage 2

A typical laser PCA run consists of about 10 sub runs. With an occupancy of 5-7% this translates into about 170,000 events. Since there is not enough 'high' charge data for an individual PMT in such a run to define the high charge tail of the walk we do a second pass over the data where we construct a global Q versus T two dimensional histogram summed over all channels. The reason why this this is even meaningful is that most of the time shifts are taken out in pass one and that the charge gains are fairly similar. Figure 5 shows the summed Q v T data in profile histogram form. The solid line shows a fit to the data. This fit is done in two stages - first we fit a polynomial of form :

$$u_0 + u_1 \times (Q - Q_m) + u_2 \times (Q - Q_m)^2 \tag{2}$$

to the 'high' charge tail (currently defined as $Q_m < Q < 850$) . Second we fit the 'low' charge part ($Q < Q_m$) to the analytic continuation of (2) plus a function of form :

$$p_0 \times \exp(-v_0 \times (Q - Q_0) - v_1 \times (Q - Q_0)^2) \tag{3}$$

In other words : the first fit will determine u_0, u_1 and u_2 which are then held constant during the second fit which determines p_0, v_0, v_1 and Q_0 . Q_m is the point at which the two functions are matched (currently set to 150). Doing the fit in two stages improves the stability of the fit.

The 7 parameters (u_0, u_1, u_2, v_0, v_1, p_0 and Q_0 now describe a *global* walk correction which is then in turn fitted to each individual channel by allowing it to slide in either Q or T within predetermined limits but *not* changing its shape. This is strictly speaking only valid if all PMTs have the same gain and similar discriminators but in practise it works well. Since there are only two free parameters for each channel we are almost guaranteed a reasonable fit even for channels with poor statistics. There is little danger of the fit being distorted at higher charge where the statistics is usually poor for any individual channel. Once 'anchored, at the 0 to 5 pe range we in effect use the average shape of the tail to predict the walk for high values of Q. We do not need to know the exact shape for high Q for an individual channel since the curve on average becomes very flat and the sensitivity goes down. For vey high charge ($Q_{hs} > 900$) we simply *define* the walk to be the walk at 900. Figure 6 shows the fit for channel 809 (1/9/9) .

Finally we do a visual inspection of the individual fits. The code drops into a ROOT browser which will display Q v T for each FEC (32 channels) . This browser can be run simultaneously with the stage 1 browser described earlier allowing a thorough inspection of all problem channels. The results of the fits (2 parameters plus one status word per channel plus the 7 parameters describing the global fit) are all written to a 'PPCA' titles file.

In this PCA we use a lower Q_{hs} cutoff. As long as this cutoff is smaller than the effective hardware threshold its exact value should not influence any subsequent analysis by very much. The justification for using a charge cut is that if one looks at the Q - T scatter plot summed over the whole detector there is a separate 'blob' which is not part of the main distribution. It is 10 ns late and has a pedestal corrected charge close to zero. It is most likely due to pickup. In addition, when looking at the fits for the individual channels it is obvious that there is other un-physical behaviour very close to or below the hardware threshold even for good channels (time would have to run backwards ocasionally etc.) so that fitting to any reasonable shape is impossible and even extrapolating is doubtful. It makes much more sense to put a charge cut on the data thereby rejecting hits we cannot time calibrate reliably. In the present PCA the charge cut was set at 8 counts above the pedestal on Q_{hs}. Going to a lower value is not possible on a global scale - the fitting simply blows up and the visual inspection of the 9300+ fits supports this conclusion. The fits generally extends to the lowest well behaved data point. It may be possible to lower the charge cut on a few hundred channels by one or two counts but it doesn't seem to be worth the effort.

As mentioned earlier the PMT gains are quite uniform across the whole detector. This means that we can employ a 'global' charge cut rather than individual ones. Since the average SPE gain is about 30 the software threshold is approximately 0.27 SPE which is not unreasonable considering the hardware thresholds are somewhere between 0.25 and 0.33 .

The visual inspection also reveals a number of channels (30 to 50) where the fit is 'bad' for one reason or another. These channel numbers are written to a separate titles file ('CHCS') so that they can be excluded when calibrating

(the PCA code returns -9997 for these marked channels) . At present we have a number of PCA laser runs and it obvious that some channels are repeat offenders. A number of these are channel 7's on a FEC. They often have multiple peaks in Q v T as if there are several classes of triggers (figure 7) . Figure 8 shows the corresponding Q_{hs} histogram. The double peaking could be due to either synchronous noise or perhaps a difference between even and odd cell TACs. Other failures are due to a discrepancy between the charge pedestal as determined from the ECA data and the laser data. Differences of up to 50 counts (about 2 pe) are not uncommon (figures 9 and 10) . It is not yet known why such pedestal shifts occur. Presumably they also occur the other way around with the laser pedestal below the ECA pedestal which would result in the channel being rejected as a 'low' or '0' occupancy channel. Yet other failures are due to double peaking in the TAC spectra (figures 11, 12 and 13) . Some of these problems may be fixable in 'software' in this PCA by simply raising the charge cut for the offending channels but others are clearly not. No attempt has been made to date to do this. The gain from fixing these channels in software is small though (an extra 5 to 10 channels) .

The PCA procedure as described above has one flaw - it depends on accurately knowing where the laserball is during the PCA run. The manipulator system works in acrylic vessel coordinates and it is known that the PSUP and AV centers differ. However, if the laserball is near the center we can take the data used to generate the PCA, create a histogram for each PMT of the PCA corrected time residual and find the difference between the prompt peak and the PSUP reflection peak. If this time difference is histogrammed as a function of the PMT x, y or z-coordinate one should get a line with slope of zero (the histogram contains the difference in time between prompt light hitting a PMT and light emitted at 180^0 reflecting off the PSUP and ending up in the *same* PMT) . Any deviation from zero slope indicates that the laserball was not in the center and the slope is related to the distance from the center. Figure 14 shows the z-histogram both as a scatter plot and as a profile histogram. The deviations below z = -600 are due to the neck of the laserball distorting the average pathlength. Reflections from near the top of the PSUP are removed thereby reducing the average reflection time. The solid angle of the acrylic vessel neck is much smaller and is not visible in this plot. The solid line is a straight line fit to the data and suggests that the laserball in this case was high by about 1.8 cm. No attempt was made to correct for this offset. The x and y-histograms do not show any distortion due to optics for this run indicating that the ball was centered in x-y .

LaserBall Reconstruction

The PCA calibrations described above has been used to analyze the both the October 1999 and the February 2000 laser runs and the results will be discussed in the following.

For the October data we used run 5599 as the PCA run and for the February one we used 10988 . Both were 500 nm runs at about 5% occupancy intended to be in the center. In most of what follows we will discuss the latter. One difference bewteen the two sets is that the manipulator source positions for the February runs were taken from the *first* CAST bank in the ZDAB file. For the October run the positions were taken from the Shift Reports because the CAST banks did not contain valid data. Since the numbers are typed into the Shift Reports they are subject to errors. The CAST banks on the other hand are written into the datastream automatically every minute or so during long runs the position values fluctuate by something like ± 1.5 mm . These variations in position are not well understood at the moment. They may be caused by variations in the rope tension or they may be caused by the acrylic vessel locatiion monitoring system.

Up to 20,000 events were fitted for each position with a time fitter based on the old Queen's Monte Carlo fitter. The final time window was tweaked to better reflect reality (the transit time averaged over the detector is more like 1.8 ns than 1.6) . It currently uses the same light speed for both H_2O and D_2O . Effective refractive indices of 1.355 and 1.385 were used at 500 and 365 nm respectively.

Histograms of the reconstructed x, y and z-distributions for a typical 500 nm run (11086) are shown in figure 15 . The source position was at (140.3, 1.2, -141.5) . A profile histogram of distance to the PMT versus time residual is shown in figure 16 .

Results for runs 11988 to 11265 (February 2000) are presented in tables 1 through 7 . The tables list run number, fitted laserball position ($\vec{r}_{fit}$), manipulator position ($\vec{r}_m$), fit radius ($|\vec{r}_{fit}|$), deviation ($|\vec{r}_{fit} - \vec{r}_{man}|$) and the cosine of the angle between $\vec{r}_{man}$ and $\vec{r}_{fit} - \vec{r}_m$. The numbers in () are the RMS of the x, y and z distributions.

For the majority of the runs there is good agreement between the manipulator position and reconstructed laserball position. There are a few cases where this is not true such as for runs 11076 and 11078. There is no obvious cause for this discrepancy and subsequent runs do reconstruct close the where they should, indicating that the problem is not due to slippage of the sideropes. The largest other deviation is for runs 11259 and 11260. The laserball was retracted, the sideropes recalibrated and the laserball was rotated between sets of runs. The most likely cause for the large deviation is a poor tension calibration of the sideropes. Fortunately there is a simple way to check if the sideropes are calibrated correctly by placing the laserball in the center and checking that the 180^0 reflection timing is independent of direction. Any time the laserball is deployed it is therefore prudent to do periodic runs in the center.

A few entries in the tables are marked 'skewed t distribution' . This refers to the distribution of reconstructed time (the fitter finds (x,y,z,t)) . Run 11086 happens to be one of the marked runs and the t distribution is shown in figure 17 . The distribution is quite narrrow indicating that the fitter does not produce outliers for the laserball at these light levels. The distribution has an RMS of 0.20 ns corresponding to a σ_R of 4.5 cm in agreement with the

RMS from the x, y and z distributions. For Čerenkov light the t distribution is dominated by the contribution from the push/pull along the fitted direction. Since this distribution in general is not symmetric one expects tails in the t distribution for Čerenkov events. However, the laserball is quite isotropic (less than 1%) and the light should not have a preferred direction for events with only 500 hit tubes hence it is not obvious why a few dozen events get shifted ealier by a about a nanosecond for a few of the laser runs.

The next set of tables lists the data for the October laserball runs. For these runs the intensity was switched between 5 and 30% at each source position. This data was presented at the Analysis Meeting in Sudbury in February and it was reported that there was a systematic shift away from the center for all the reconstructed poistions but no shifts with changes of intensity. Subsequent re-analysis has shown the systematic shifts were caused by a light speed problem in the fitter (one part of the fitter used a hardwired speed of light rather than the value read in ...)

This 'error' highlighted a general fitter problem : the fitted position depends on the light speed used in that distance from the center scales with c. A 1% error in c leads to a 1% in radius or a 3% error in fiucial volume. Čerenkov light has a broad wavelength distribution and will have to be fit with a suitably choosen refractive index and the broad distribution will contribute to the uncertainty in the reconstruction. Furthermore, it will be position and direction dependent since the wavelength distribution is distorted by optically active components in the detector.

The re-analyzed data from October is shown in tables 8 to 11 . Again the agreement between the reconstructed and manipulator positions is generally good. The deviation for run 5858 has to be due to an incorrect recording of the source position in the Shift Report (due to a bug in the DAQ code there were unfortunately no valid CAST banks) . The only other large discrepancy is for runs 5976 and 5977 but as for the February runs there is no obvious reason.

From the data presented above it is reasonable to conclude that in general there is good agreement between the reconstructed laserball position and the source position given by the manipulator system. Furthermore, the laserball reconstructed positions are independent of laser wavelength and they do not move significantly when the light intensity is changed. We can therefore conclude that the PCA presented here works correctly for average occupancies of up to about 30% .

Further work

An investigation of why some channels appear to have a different pedestal laser and electronic pedestal is underway. Also underway is an estimate of how much the H_2O/D_2O difference in refrative index affects the fitter.

Since this PCA gives an estimate of the SPE gain it is probably worth looking at the last PCA run done before we raised the high voltage and getting an independent number for the increase in gain.

Finallly, since this PCA imposes a charge cut it will affect the 'energy' calibration at least for prompt light. A detailed study of N_{hit} - N_{cal} and how it is broken down (failed ECA, failed PCA, ...) needs to be done.

Run	x_{fit}	y_{fit}	z_{fit}	x_{man}	y_{man}	z_{man}	λ	r_{fit}	δr	δcos
10988	-0.7(3.9)	0.5(3.9)	0.4(4.1)	-0.3	0.8	0.0	500	0.9	0.6	-0.219
10990	0.5(4.1)	1.5(4.1)	0.6(4.4)	-0.3	-0.8	0.1	365	1.7	2.5	-0.949
10993	0.4(4.3)	2.7(4.3)	-552.5(4.7)	-0.1	1.4	-552.2	365	552.5	1.4	0.213
10995	0.7(6.6)	2.2(6.3)	-552.8(5.6)	-0.0	1.3	-552.2	500^1	552.8	1.3	0.467
10996	-0.4(3.9)	2.6(3.9)	-553.4(4.3)	0.1	1.4	-552.2	500	553.4	1.8	0.680
10998	0.9(3.9)	1.9(3.9)	-500.9(4.2)	0.3	1.4	-502.2	500	500.9	1.5	-0.856
11000	1.5(4.5)	2.2(4.5)	-500.1(4.9)	0.3	1.5	-502.2	365	500.1	2.5	-0.833
11002	1.0(4.6)	1.9(4.6)	-397.5(5.0)	0.4	1.4	-399.9	365	397.5	2.5	-0.950
11004	-0.1(4.1)	2.0(4.1)	-398.7(4.3)	0.3	1.4	-399.9	500	398.7	1.4	-0.856
11006	-0.9(4.2)	1.6(4.2)	-199.2(4.4)	-0.3	1.0	-200.0	500	199.2	1.2	-0.683
11008	-0.0(4.8)	1.8(4.8)	-198.7(5.2)	-0.3	1.1	-200.0	365	198.7	1.5	-0.861
11010	-0.3(4.8)	0.4(4.9)	201.0(5.1)	-0.2	0.7	200.2	365	201.0	0.9	0.929
11012	-0.4(4.2)	0.4(4.2)	200.1(4.4)	-0.2	0.8	200.3	500	200.1	0.5	-0.411
11014	-0.3(4.1)	0.4(4.1)	399.0(4.5)	0.1	0.9	400.1	500	399.0	1.3	-0.865
11016	0.4(4.8)	0.7(4.8)	399.7(5.4)	0.1	0.8	400.5	365	399.7	0.9	-0.930
11018	0.3(4.9)	0.5(5.0)	498.0(6.0)	-0.3	0.8	500.1	365	498.0	2.2	-0.953
11020	-0.1(4.2)	-0.0(4.3)	497.6(4.8)	-0.3	0.8	500.4	500	497.6	2.9	-0.960
11023	-5.5(4.4)	12.5(4.6)	552.5(5.2)	-7.6	12.9	549.9	500	552.7	3.4	0.761
11025	-5.3(5.9)	12.5(6.1)	548.7(8.1)	-7.3	12.9	549.9	365	548.9	2.4	-0.522
11027	-0.3(5.4)	1.0(5.5)	0.5(5.8)	-0.1	0.7	-0.1	365^t	1.2	0.7	0.340

Table 1: Vertical (z) scan. [1] Long tails on t (fitted time) distribution. [t] Skewed t distribution.

Run	x_{fit}	y_{fit}	z_{fit}	x_{man}	y_{man}	z_{man}	λ	r_{fit}	δr	δcos
11030	-0.2(4.0)	1.0(4.0)	-0.7(4.1)	-0.1	0.7	-0.1	500	1.2	0.7	0.578
11032	-200.7(4.2)	0.2(4.1)	0.6(4.2)	-199.1	0.7	-0.1	500	200.7	1.8	0.880
11038	-199.5(3.9)	0.9(3.8)	1.0(4.0)	-199.0	0.8	-0.1	365	199.5	1.2	0.412
11040	-399.6(4.0)	0.3(3.9)	1.7(4.1)	-397.2	-0.1	-0.9	365	399.6	3.6	0.672
11042	-399.0(4.9)	-0.4(4.7)	1.4(4.9)	-397.2	-0.1	-0.9	500	399.0	2.9	0.611
11044	-486.7(5.2)	-0.4(4.8)	5.0(5.1)	-483.2	-0.6	1.9	500	486.7	4.7	0.750
11046	-485.8(5.8)	0.4(5.5)	5.2(5.8)	-483.2	-0.6	1.9	365^1	485.8	4.3	0.605
11048	200.6(5.2)	0.7(5.2)	0.3(5.4)	199.0	0.7	-0.1	365	200.6	1.6	0.970
11050	199.6(4.8)	0.2(4.8)	-0.5(5.0)	199.4	0.8	-0.1	500	199.6	0.7	0.264
11052	398.7(4.9)	-0.2(4.7)	-0.1(4.8)	397.9	-0.3	-0.6	500^t	398.7	0.9	0.842
11054	399.7(5.5)	-0.7(5.4)	0.9(5.7)	397.9	-0.3	-0.5	365	399.7	2.3	0.777
11056	488.7(5.6)	-0.3(5.5)	2.1(5.8)	486.4	-0.7	0.8	365	488.7	2.7	0.861
11058	484.4(4.8)	-0.5(4.7)	-0.7(4.9)	483.0	-0.8	-1.1	500	484.4	1.5	0.941

Table 2: Horizontal (x) scan. [1] Many GTID=0x0 events, broad N_{hit} distribution. [t] Skewed t distribution.

Run	x_{fit}	y_{fit}	z_{fit}	x_{man}	y_{man}	z_{man}	λ	r_{fit}	δr	δcos
11060	233.7(4.8)	-0.4(4.7)	231.3(5.0)	236.0	0.2	236.4	500^t	328.8	5.6	-0.930
11062	234.5(6.0)	-0.3(6.0)	232.0(6.3)	236.2	0.2	236.6	365	329.9	4.9	-0.904
11064	139.5(5.5)	0.1(5.5)	139.1(5.9)	140.7	0.8	141.3	365	197.0	2.6	-0.926
11066	138.9(3.7)	-0.2(3.6)	138.6(3.8)	140.6	0.9	141.0	500	196.2	3.1	-0.925
11068	-141.3(4.5)	1.4(4.4)	-141.1(4.8)	-140.1	1.2	-141.5	500^t	199.7	1.3	0.438
11070	-140.5(5.3)	1.8(5.2)	-140.8(5.6)	-140.1	1.3	-141.5	365	198.9	0.9	-0.224
11072	-280.3(5.1)	2.1(5.0)	-282.3(5.5)	-277.6	1.4	-283.7	365	397.8	3.1	0.285
11074	-280.3(4.6)	1.5(4.5)	-281.9(4.8)	-277.8	1.2	-283.8	500	397.5	3.2	0.124
11076	-244.7(4.5)	0.5(4.4)	239.9(4.7)	-246.7	0.2	247.7	500	342.7	8.1	-0.861
11078	-244.5(5.8)	0.7(5.6)	240.5(6.0)	-246.7	0.2	248.1	365	343.0	7.9	-0.875
11080	280.8(5.7)	0.6(5.5)	-281.6(6.2)	277.6	1.1	-283.6	365^t	397.7	3.8	0.212
11082	280.2(4.6)	0.2(4.5)	-282.1(4.8)	277.8	1.2	-283.5	500	397.6	3.0	0.229
11084	0.7(4.4)	1.4(4.4)	-0.3(4.7)	0.1	1.0	0.2	500[1]	1.6	0.9	0.400
11086	140.8(4.5)	0.9(4.4)	-141.5(4.7)	140.3	1.2	-141.5	500^t	199.6	0.6	0.601
11088	1.2(5.9)	1.7(6.0)	0.4(6.4)	-0.2	0.9	0.1	365	2.1	1.6	0.309

Table 3: Diagonal (x-z) scan. ^{t} Skewed t distribution. [1] Short run.

Run	x_{fit}	y_{fit}	z_{fit}	x_{man}	y_{man}	z_{man}	λ	r_{fit}	δr	δcos
11099	-1.0(7.5)	0.7(7.6)	-0.2(8.2)	0.1	0.6	-0.1	500[1]	1.2	1.1	-0.059
11105	-0.9(3.1)	0.8(3.1)	-0.5(3.2)	-0.0	0.7	-0.1	500	1.3	1.0	0.157
11107	-0.8(3.7)	0.9(3.8)	-0.1(3.9)	0.0	0.8	-0.1	365	1.2	0.8	0.123
11115	-1.1(4.1)	1.7(4.1)	-1.2(4.3)	-0.6	-0.1	-0.1	365[2]	2.4	2.2	0.172
11117	-1.8(3.6)	1.3(3.7)	-1.9(3.8)	-0.7	-0.2	-0.1	500	2.9	2.6	0.342
11119	-2.2(3.9)	-465.3(4.0)	-1.5(4.0)	-0.2	-463.7	0.1	500?	465.3	3.0	0.530
11122	-1.9(3.9)	-465.1(4.0)	-1.6(4.1)	-0.2	-463.6	0.1	500	465.1	2.8	0.529
11124	-1.5(5.3)	-464.3(5.9)	-1.2(5.7)	-0.2	-463.8	0.2	365	464.3	2.0	0.253
11126	-1.3(4.0)	-396.7(4.1)	-2.6(4.1)	-0.6	-397.1	-0.7	365	396.7	2.1	-0.192
11129	-1.2(4.1)	-396.5(4.2)	-2.6(4.4)	-0.6	-397.1	-0.7	365	396.5	2.1	-0.286
11131	-1.6(3.2)	-397.2(3.3)	-3.1(3.2)	-0.6	-397.0	-0.7	500	397.2	2.6	0.079
11134	-1.6(4.3)	-396.5(4.4)	-3.0(4.5)	-0.6	-397.0	-0.7	500	396.5	2.6	-0.193
11136	-1.2(4.2)	-196.7(4.3)	-2.5(4.4)	-0.9	-198.4	-0.2	500	196.7	2.9	-0.590
11138	-0.9(4.3)	-196.3(4.4)	-2.0(4.5)	-0.9	-198.4	-0.2	365	196.3	2.8	-0.759
11140	-0.6(4.6)	201.4(4.7)	0.0(5.0)	-1.0	198.6	-0.1	365	201.4	2.8	0.989
11142	-0.7(4.1)	201.0(4.2)	-0.4(4.3)	-1.0	198.6	-0.1	500	201.0	2.4	0.984
11144	-0.3(4.0)	401.1(4.1)	0.1(4.1)	-0.3	397.7	-0.7	500	401.1	3.5	0.973
11146	-0.2(3.9)	401.5(4.0)	0.6(4.1)	-0.4	397.8	-0.5	365	401.5	3.9	0.957
11148	-0.1(4.0)	451.2(4.1)	0.8(4.1)	-0.3	447.0	-0.8	365	451.2	4.5	0.933
11150	-0.3(4.1)	450.5(4.1)	0.2(4.1)	-0.2	447.1	-0.7	500	450.5	3.5	0.966

Table 4: Horizontal (y) scan. [1] Very broad N_hit distribution (Unstable laser). [2] Garbage (orphans ?) near start of run.

Run	x_{fit}	y_{fit}	z_{fit}	x_{man}	y_{man}	z_{man}	λ	r_{fit}	δr	δcos
11152	-0.1(4.0)	219.6(4.1)	218.7(4.3)	-0.4	218.4	221.0	500	309.9	2.6	-0.304
11154	0.4(4.0)	218.7(4.1)	219.1(4.3)	-0.4	217.4	220.8	365	309.6	2.3	-0.131
11156	-0.0(4.1)	141.3(4.1)	139.4(4.4)	-0.8	141.0	141.5	365	198.5	2.3	-0.564
11158	-0.2(4.0)	141.1(4.0)	138.9(4.2)	-0.8	141.0	141.4	500	198.0	2.6	-0.662
11160	-1.0(4.1)	0.4(4.2)	-2.5(4.3)	-0.7	-0.1	-0.1	500	2.7	2.5	0.227
11162	-0.8(4.4)	0.9(4.5)	-2.0(4.7)	-0.6	-0.1	-0.1	365	2.3	2.2	0.158
11164	-1.4(4.3)	-139.8(4.4)	-143.0(4.7)	-1.0	-140.8	-141.8	365^t	200.0	1.6	0.092
11166	-1.2(4.2)	-139.9(4.2)	-143.8(4.5)	-1.0	-140.6	-141.8	500	200.6	2.1	0.436
11173	-1.5(3.0)	-254.6	-260.7(3.1)	-1.1	-254.3	-259.4	500	364.4	1.4	0.8180
11175	-1.4(3.9)	-254.0(4.1)	-260.1(4.3)	-1.1	-254.3	-259.4	500	363.6	0.8	0.355
11177	-1.1(3.7)	-254.2(3.7)	-260.1(4.0)	-1.3	-254.2	-259.4	365	363.7	0.7	0.686
11182	-0.6(4.0)	0.9(3.6)	-1.3(3.4)	-0.5	-0.1	-0.1	365^t	1.7	1.6	0.086
11184	-1.5(3.0)	0.7(3.1)	-2.1(3.1)	-0.5	-0.1	-0.1	500	2.7	2.4	0.502
11189	-0.8(2.9)	282.8(3.0)	-283.4(3.0)	-1.1	277.7	-283.8	500	400.4	5.1	0.640
11191	-0.8(3.3)	282.7(3.3)	-282.6(3.4)	-1.1	277.7	-283.8	365	399.7	5.2	0.512
11193	-1.3(3.5)	142.3(3.5)	-141.4(3.7)	-1.1	140.4	-141.5	365	200.6	1.9	0.663
11195	-1.3(3.1)	142.1(3.1)	-142.0(3.2)	-1.2	140.4	-141.5	500	200.9	1.8	0.875
11197	-1.6(3.1)	1.1(3.1)	-1.8(3.3)	-0.8	-0.1	0.1	500	2.6	2.4	0.170
11199	-1.2(3.6)	1.5(3.6)	-1.0(3.8)	-0.7	-0.1	0.1	365	2.2	2.0	0.056
11201	-0.6(3.4)	-140(3.5)	139.4(3.6)	-0.7	-141.2	141.5	365	197.6	2.4	-0.964
11203	-1.0(3.3)	-140.4(3.3)	138.7(3.4)	-0.8	-141.2	141.5	500	197.4	2.9	-0.872
11205	-1.1(3.2)	-218.6(3.3)	216.9(3.3)	-0.5	-218.6	220.8	500^1	307.9	3.9	-0.702
11207	-0.7(3.0)	-218.1(3.2)	217.4(3.2)	-0.5	-218.8	221.5	365	307.9	4.2	-0.819
11209	-0.7(2.9)	-217.3(3.0)	216.6(3.0)	-0.4	-219.0	221.8	365	306.8	5.5	-0.893

Table 5: Diagonal (x-y) scan. ^{t} Skewed t distribution. ^{1} Some low N_{hit} events.

Run	x_{fit}	y_{fit}	z_{fit}	x_{man}	y_{man}	z_{man}	λ	r_{fit}	δr	δcos
11211	-7.7(3.6)	2.8(3.8)	548.1(4.8)	-8.7	-2.5	549.9	365	548.2	5.7	-0.324
11213	-7.6(4.3)	2.6(4.7)	551.3(4.9)	-8.7	-1.9	549.8	500[1]	551.4	4.9	0.301
11215	-7.6(3.9)	2.6(4.1)	551.1(4.7)	-8.6	-1.6	549.8	500	551.2	4.5	0.282
11217	-0.5(3.7)	0.9(3.8)	395.6(4.2)	-0.4	0.0	400.1	500	395.6	4.6	-0.980
11219	-0.2(3.4)	1.2(3.5)	396.6(3.8)	-0.5	-0.2	399.9	365	396.6	3.6	-0.918
11221	-1.0(3.4)	2.2(3.4)	-1.8(3.6)	-0.5	-0.0	0.1	365	3.0	2.9	0.040
11223	-1.1(3.8)	1.7(3.8)	-2.6(4.0)	-0.7	-0.1	0.1	500	3.3	3.3	-0.073
11225	-2.3(3.6)	3.2(3.7)	-400.9(4.0)	-0.9	0.3	-400.1	500	400.9	3.3	0.243
11227	-2.0(3.5)	3.5(3.7)	-400.5(3.9)	-0.9	0.2	-400.1	365	400.5	3.5	0.115
11229	-1.8(3.5)	3.0(3.5)	-201.3(3.7)	-0.9	0.0	-200.0	365	201.3	3.4	0.385
11230	-1.7(3.5)	2.9(3.5)	-201.4(3.6)	-0.8	0.1	-200.0	365	201.4	3.3	0.431
11232	-2.0(3.8)	2.7(3.8)	-201.9(4.0)	-0.9	0.0	-200.0	500	201.9	3.5	0.547
11234	-1.2(3.7)	2.3(3.9)	-2.5(4.1)	-0.7	0.1	0.1	500	3.6	3.4	0.126
11236	-1.0(3.9)	2.7(3.9)	-1.9(4.0)	-0.9	0.2	0.1	365	3.4	3.2	0.131
11238	-0.7(3.8)	2.4(3.9)	197.2(4.0)	-0.7	0.0	200.1	365	197.2	3.8	-0.770
11240	-1.2(3.9)	1.7(3.9)	196.5(4.2)	-0.7	-0.0	200.2	500	196.5	4.1	-0.901
11242	-0.8(4.2)	1.7(4.2)	494.9(5.1)	-0.3	-0.1	500.8	365	494.9	6.2	-0.953
11244	-0.6(4.1)	1.2(4.1)	494.4(4.6)	-0.4	-0.1	501.2	500	494.4	6.9	-0.982

Table 6: Vertical (z) scan. [t] Skewed t distribution. [1] Some late t events.

Run	x_{fit}	y_{fit}	z_{fit}	x_{man}	y_{man}	z_{man}	λ	Dir.	r_{fit}	δr	δcos
11250	-0.1(3.7)	0.8(3.7)	-0.0(3.9)	0.0	0.8	-0.2	500	S	0.8	0.2	-0.217
11252	1.2(4.7)	1.5(4.7)	0.4(5.0)	0.1	0.8	-0.2	365	S	2.0	1.4	0.461
11255	-1.1(3.9)	3.2(3.8)	0.7(4.0)	-0.0	0.8	-0.1	500	N	3.5	2.8	0.827
11259	-9.6(4.0)	0.9(4.0)	-1.1(4.2)	-0.7	-0.3	-0.3	500	W	9.7	9.0	0.828
11260	-9.0(4.0)	0.9(4.1)	-1.4(4.2)	-0.7	-0.2	-0.4	500	W	9.2	8.4	0.855
11263	-1.4(4.1)	-0.1(4.2)	-3.0(4.3)	-0.8	0.1	-0.1	500	E	3.3	3.0	0.311
11265	-1.4(4.1)	0.4(4.1)	-1.4(4.4)	-0.8	0.0	-0.1	337	E	2.0	1.5	0.509

Table 7: Flipped laserball runs. Column 9 lists the orientation of the slot.

Run	x_{fit}	y_{fit}	z_{fit}	Occ.	x_{man}	y_{man}	z_{man}	r_{fit}	δr	δcos
5798	-0.9(3.6)	1.6(3.5)	0.3(3.6)	5	0.2	0.8	-0.1	1.9	1.4	0.323
5800	-0.6(3.6)	0.8(3.6)	400.7(3.9)	5	0.1	0.8	400.4	400.7	0.8	0.394
5802	-1.0(1.8)	0.3(1.7)	402.1(1.7)	35	0.0	0.9	400.6	402.1	1.9	0.789
5805	-1.5(1.6)	1.0(1.6)	0.0(1.5)	35	0.0	0.6	-0.1	1.8	1.6	0.243
5807	-1.2(3.8)	1.4(3.7)	-0.0(3.9)	5	0.1	0.6	-0.1	1.8	1.5	0.361
5808	-0.7(3.5)	2.3(3.5)	-398.8(4.0)	5	0.3	1.1	-400.0	398.8	2.0	-0.608
5810	-1.0(1.7)	1.7(1.6)	-401.3(1.7)	35	0.3	1.2	-400.0	401.3	1.9	0.683
5812	-1.8(1.6)	1.2(1.6)	0.6(1.4)	35	0.6	1.0	0.1	2.2	2.5	-0.413
5814	-1.5(3.6)	1.7(3.7)	0.5(3.8)	5	0.0	1.0	0.1	2.3	1.7	0.432
5816	-1.9(3.7)	2.1(3.7)	-199.6(3.9)	5	-0.1	0.8	-200.1	199.6	2.3	-0.217
5817	-2.1(1.7)	1.6(1.7)	-200.2(1.7)	35	0.0	0.9	-200.1	200.2	2.2	0.047
5819	-1.7(1.8)	1.2(1.7)	0.7(1.6)	35	0.0	0.8	0.1	2.2	1.8	0.255
5821	-1.4(3.8)	1.7(3.7)	0.6(3.9)	5	0.0	0.8	0.1	2.3	1.7	0.550

Table 8: Vertical (z) scan.

Run	x_{fit}	y_{fit}	z_{fit}	Occ.	x_{man}	y_{man}	z_{man}	r_{fit}	δr	δcos
5836	-1.5(1.6)	1.7(1.6)	0.7(1.5)	33	-0.1	0.8	0.1	2.4	1.8	0.640
5839	-1.6(3.8)	1.8(3.7)	0.7(3.9)	6	-0.1	0.8	0.1	2.5	1.9	0.654
5840	-1.2(4.0)	1.2(3.9)	201.0(4.2)	6	0.0	0.8	200.4	201.0	1.4	0.430
5842	-1.1(1.7)	1.2(1.6)	201.9(1.5)	33	0.0	0.8	200.4	201.9	1.9	0.789
5843	-1.6(1.7)	1.6(1.7)	0.5(1.5)	33	0.1	0.8	-0.1	2.3	2.0	0.256
5845	-1.8(3.7)	1.6(3.7)	0.5(3.8)	6	0.1	0.8	-0.1	2.5	2.1	0.224
5847	-1.9(3.9)	2.0(4.0)	-299.0(4.1)	6	-0.1	1.0	-300.0	299.0	2.3	-0.435
5848	-1.9(1.8)	2.0(1.7)	-300.5(1.6)	33	-0.1	1.0	-300.0	300.5	2.1	0.238
5851	-1.9(3.7)	1.7(3.6)	0.8(3.8)	6	0	0	0[1]	2.7	2.7	0.000
5853	-1.8(3.9)	0.5(3.9)	300.9(4.2)	6	0.0	0.8	300.4	300.9	1.9	0.264
5855	-1.9(1.7)	0.6(1.7)	302.2(1.6)	33	0.0	0.8	300.4	302.2	2.6	0.686
5856	-2.1(1.7)	1.2(1.7)	0.5(1.6)	33	0.1	0.7	-0.0	2.5	2.3	0.080
5857	-1.8(9.8)	1.2(8.1)	0.9(9.8)	6	0.1	0.7	-0.0	2.3	2.2	0.105
5858	-2.2(3.9)	1.2(3.8)	0.5(4.0)	6	0.3	1.1	-400.0	2.6	400.5[2]	-1.000
5859	-2.4(3.9)	1.8(3.9)	-398.0(4.5)	6	0.3	1.1	-400.0	398.0	3.4	-0.583
5861	2.3(1.8)	1.8(1.8)	-400.1(1.8)	33	0.2	1.2	-400.0	400.1	2.2	0.047
5863	-2.3(2.1)	1.3(1.9)	0.9(1.8)	33	0.0	0.9	0.2	2.8	2.4	0.223
5867	-2.4(4.1)	1.4(4.1)	1.0(4.3)	6	0.0	0.9	0.2	3.0	2.6	0.257

Table 9: Vertical (z) scan. [1] Actual position not recorded in Shift Report. [2] This position is likely recorded wrong in the Shift Report. [3] Unstable laser, low statistics and many low N_{hit} events.

Run	x_{fit}	y_{fit}	z_{fit}	λ	Occ.	x_{man}	y_{man}	z_{man}	r_{fit}	δr	δcos
5875	-1.9(4.1)	1.8(4.1)	0.9(4.3)	500	5	0.1	0.9	0.2	2.8	2.3	0.351
5877	-1.6(4.1)	2.0(4.0)	1.2(4.3)	421	5	0.0	0.8	0.2	2.8	2.2	0.629
5884	-1.3(3.3)	2.2(3.2)	1.3(3.4)	386	5	0.0	0.9	0.2	2.9	2.1	0.704
5886	-1.3(3.7)	2.3(3.6)	1.6(3.9)	365	5	0.1	1.0	0.2	3.1	2.4	0.593
5888	-0.8(6.5)	2.6(6.3)	3.5(6.9)	337	5	0.1	1.0	0.2	4.4	3.8	0.561

Table 10: Wavelength scan at center

Run	x_{fit}	y_{fit}	z_{fit}	Occ.	x_{man}	y_{man}	z_{man}	r_{fit}	δr	δcos
5926	-2.1(4.0)	1.4(4.0)	1.5(4.2)	5	0.1	0.8	-0.1	2.9	2.8	0.044
5929	-2.4(1.7)	0.9(1.6)	1.5(1.5)	30	0.1	-.8	-0.1	3.0	3.4	-0.637
5932	59.8(3.9)	1.0(4.0)	80.6(4.1)	6	61.5	0.9	78.9	100.4	2.4	0.123
5934	-277.7(4.4)	1.7(4.3)	-355.0(4.4)	5	-273.0	1.7	-358.0	450.7	5.6	0.083
5936	-279.2	1.5(1.7)	-357.3(1.7)	30	-272.8	1.6	-358.1	453.5	6.5	0.503
5942	-245.6(4.1)	1.4(3.9)	-313.1(4.2)	5	-241.7	1.5	-315.3	397.9	4.5	0.140
5944	-246.8(1.9)	1.1(1.7)	-314.6(1.7)	30	-249.4	1.6	-315.8	399.9	2.9	-0.879
5946	181.2(4.0)	-0.6(3.9)	236.6(4.2)	5	183.9	0.6	236.1	298.0 [1]	3.0	-0.423
5948	181.6(1.8)	-1.2(1.7)	237.3(1.6)	30	183.9	0.6	236.2	298.8	3.1	-0.176
5950	-125.7(4.0)	1.2(4.0)	-155.9(4.1)	5	-121.9	1.4	-157.7	200.3	4.2	0.214
5952	-126.1(1.8)	0.8(1.7)	-156.5(1.6)	30	-121.9	1.3	-157.7	201.0	4.4	0.368
5954	-3.1(1.8)	0.7(1.7)	1.6(1.6)	30	0.0	0.9	0.2	3.6	3.4	0.032
5956	-2.8(3.9)	1.2(3.9)	1.5(4.0)	5	0.0	0.9	0.2	3.4	3.1	0.185
5964	-2.6(3.8)	1.2(3.8)	1.7(4.0)	5	-0.0	0.9	0.2	3.3	3.0	0.205
5968	202.4(1.6)	-0.6(1.6)	265.2(1.5)	30	203.1	0.4	259.4	333.6	5.9	0.697
5970	200.7(3.8)	-0.8(3.7)	264.2(3.7)	5	203.1	0.4	259.4	331.8	5.5	0.418
5972	-4.2(2.2)	0.4(4.1)	2.3(4.1)	5	-0.4	0.7	-0.1	4.8	4.5	0.292
5974	-3.6(1.6)	0.7(1.6)	2.0(1.5)	30	-0.5	0.6	-0.0	4.2	3.7	0.559
5976	-305.3(1.9)	1.6(1.7)	-387.1(1.7)	30	-296.2	1.5	-387.8	493.0	9.1	0.544
5977	-303.7(3.9)	1.6(3.8)	-384.4(3.9)	5	-296.3	1.6	-387.8	489.9	8.1	0.220
5978	-3.1(3.9)	1.0(4.0)	3.1(4.0)	5	0.2	1.0	0.2	4.5	4.4	-0.018
5980	-3.0(1.7)	1.0(1.6)	2.9(1.5)	30	0.1	0.9	0.2	4.3	4.1	0.084
5982	89.8(1.7)	0.3(1.7)	121.9(1.7)	30	92.1	1.0	118.4	151.4	4.2	0.317
5984	89.3(3.9)	0.3(3.8)	121.6(4.0)	5	92.1	1.0	118.4	150.9	4.3	0.186
5986	-3.5(3.9)	0.9(3.8)	2.7(4.0)	5	0.2	0.9	-0.2	4.5	4.7	-0.298
5988	-3.3(1.7)	0.9(1.7)	2.6(1.6)	30	0.1	0.8	-0.2	4.3	4.4	-0.224

Table 11: Diagonal (x-z) scan. [1] Recorded wrong in Shift Report. [2] No DQXX file - used previous run. [3] No ASYNC - used N_{hit} trigger.

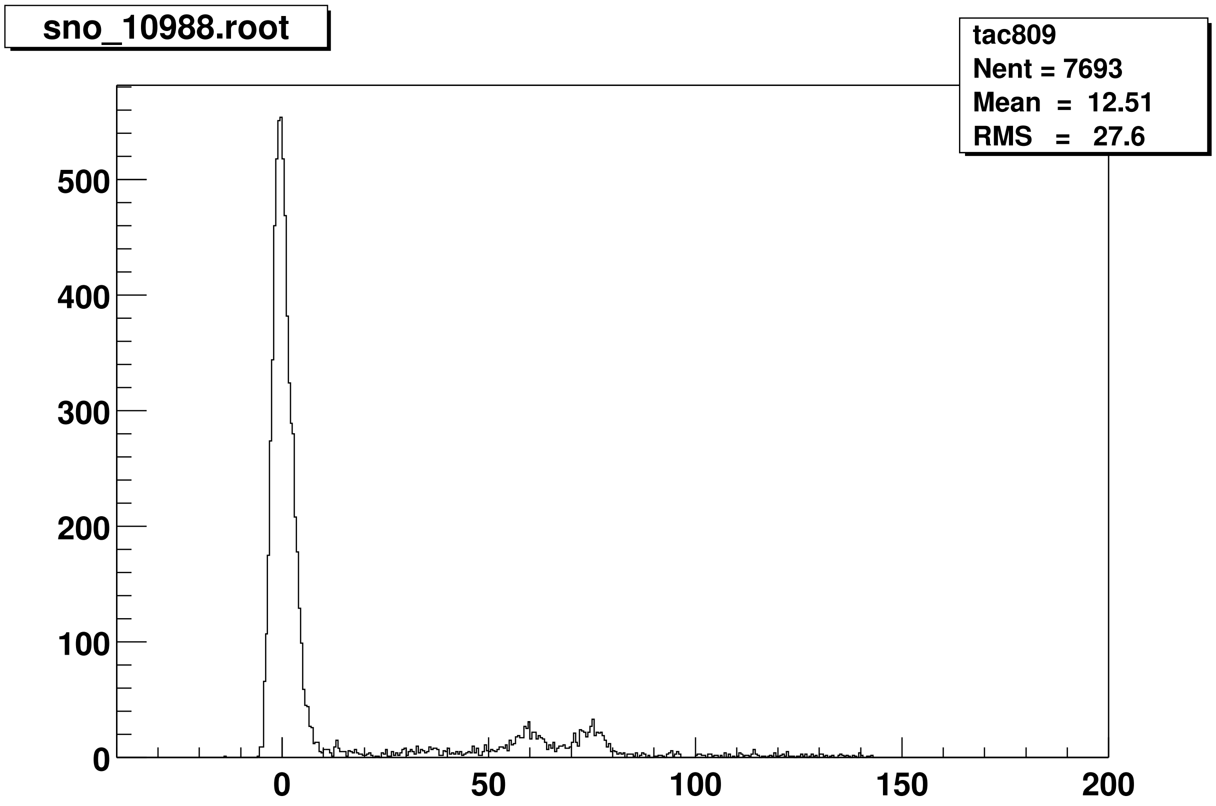

Figure 1: Figure 1. Time residual histogram for channel 1/9/9

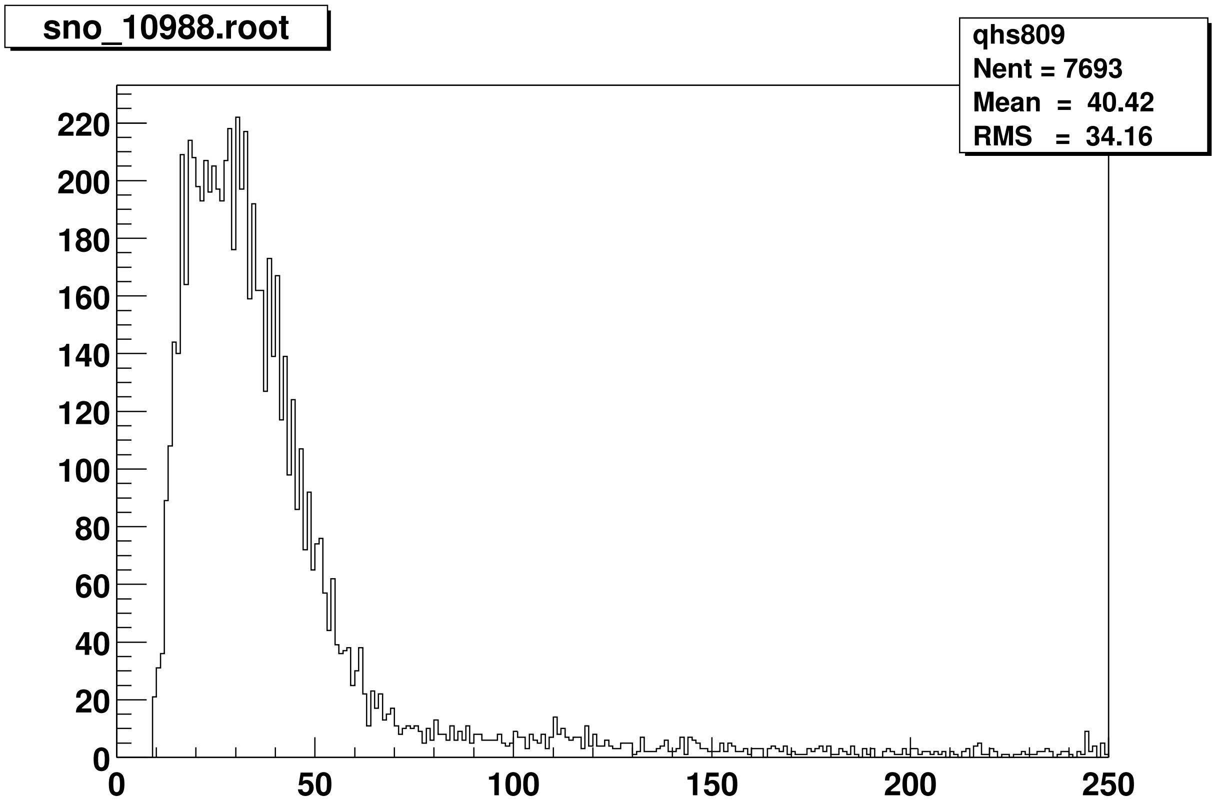

Figure 2: Figure 2. Charge (Q_{hs}) histogram for channel 1/9/9

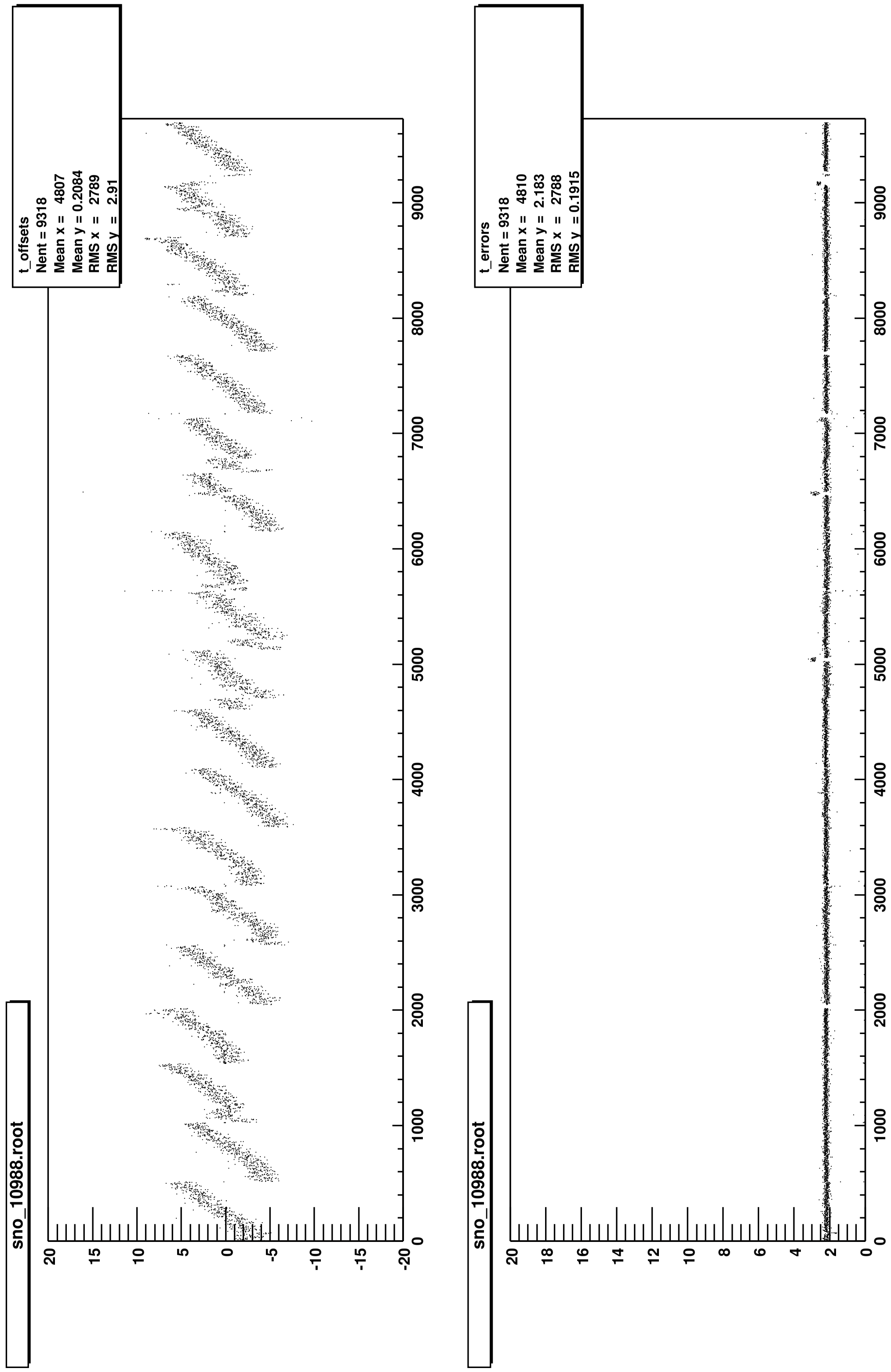

Figure 3: Figure 3. Average walk in nanoseconds as a function of channel number (top panel) and RMS of walk (bottom panel).

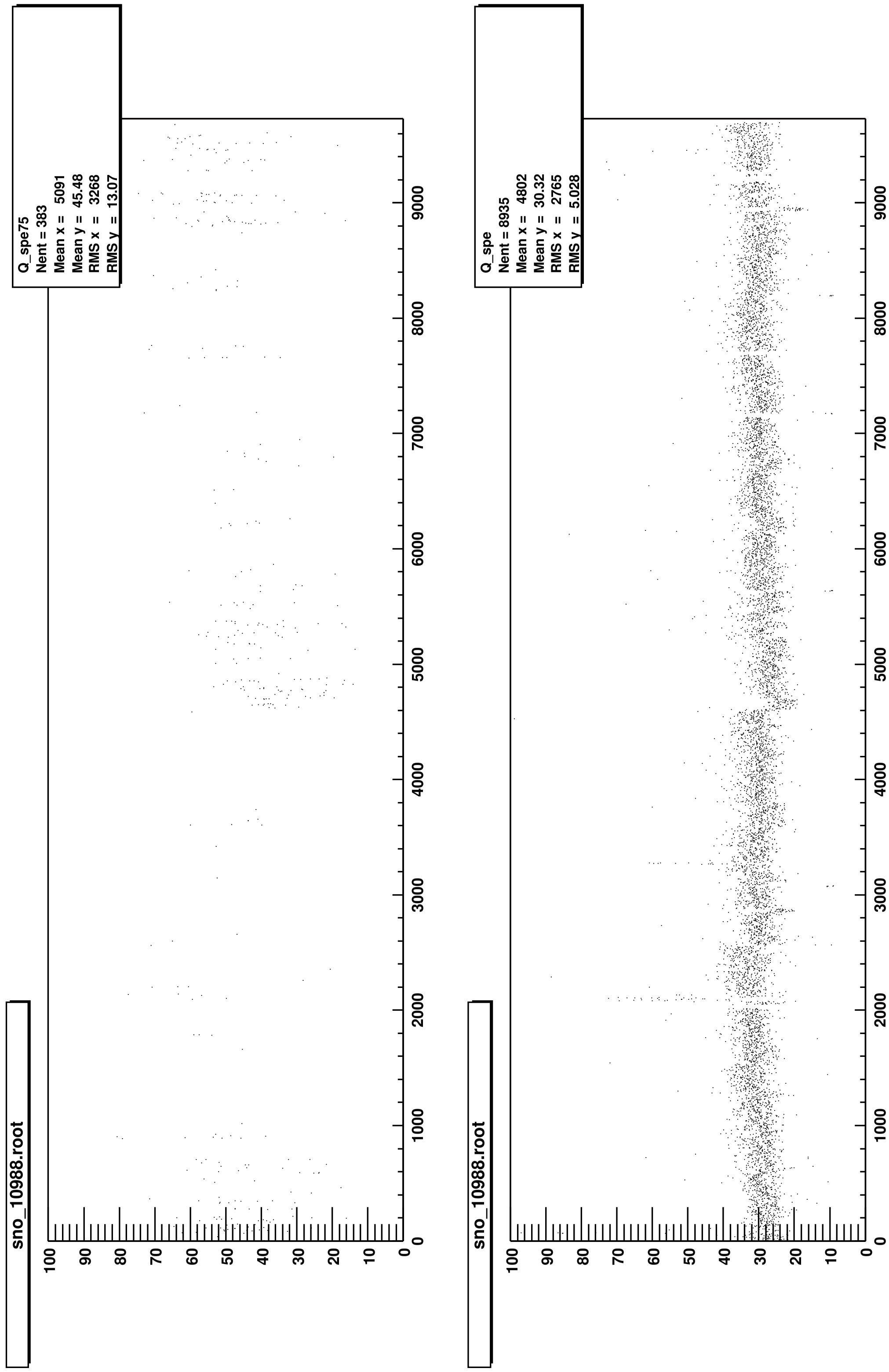

Figure 4: Figure 4. Single photon electron (SPE) gain (Q_{hs}) as function of channel number for channels with blown 75Ω (top panel) and intact 75Ω terminators (bottom panl) .

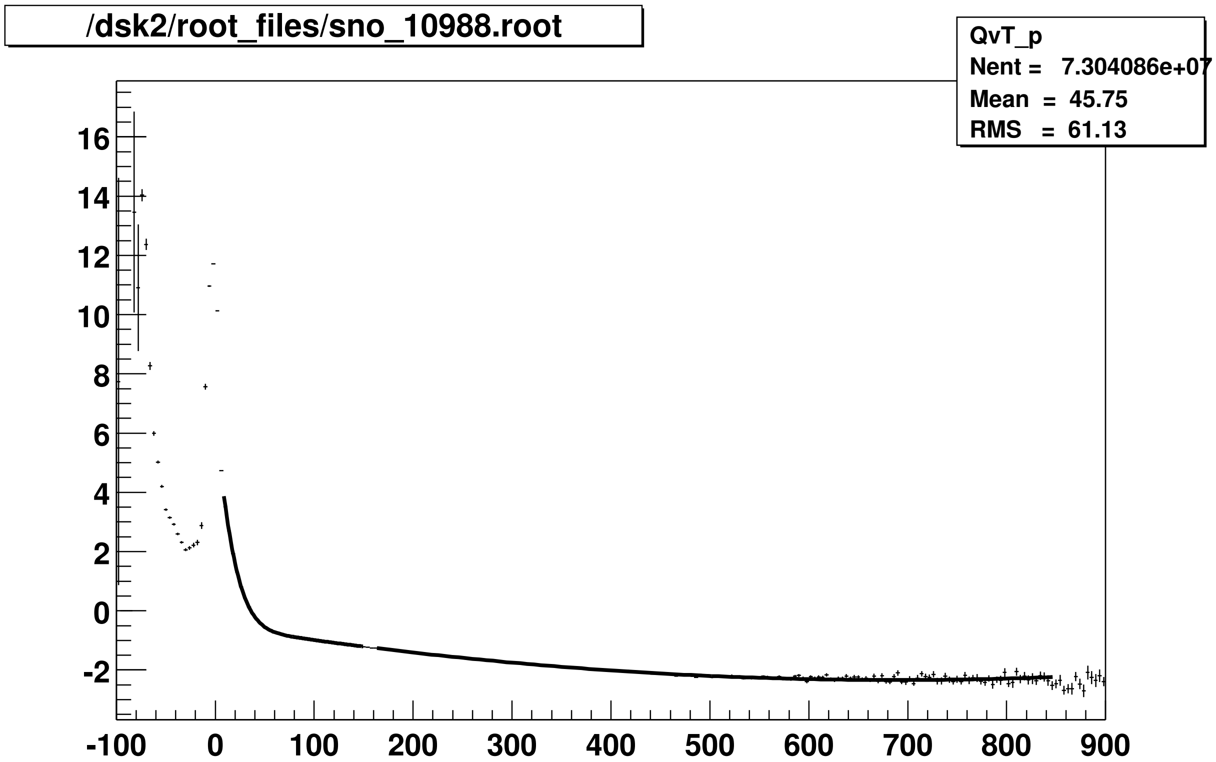

Figure 5: Figure 5. Q versus T averaged over all channels. The solid line shows the fit.

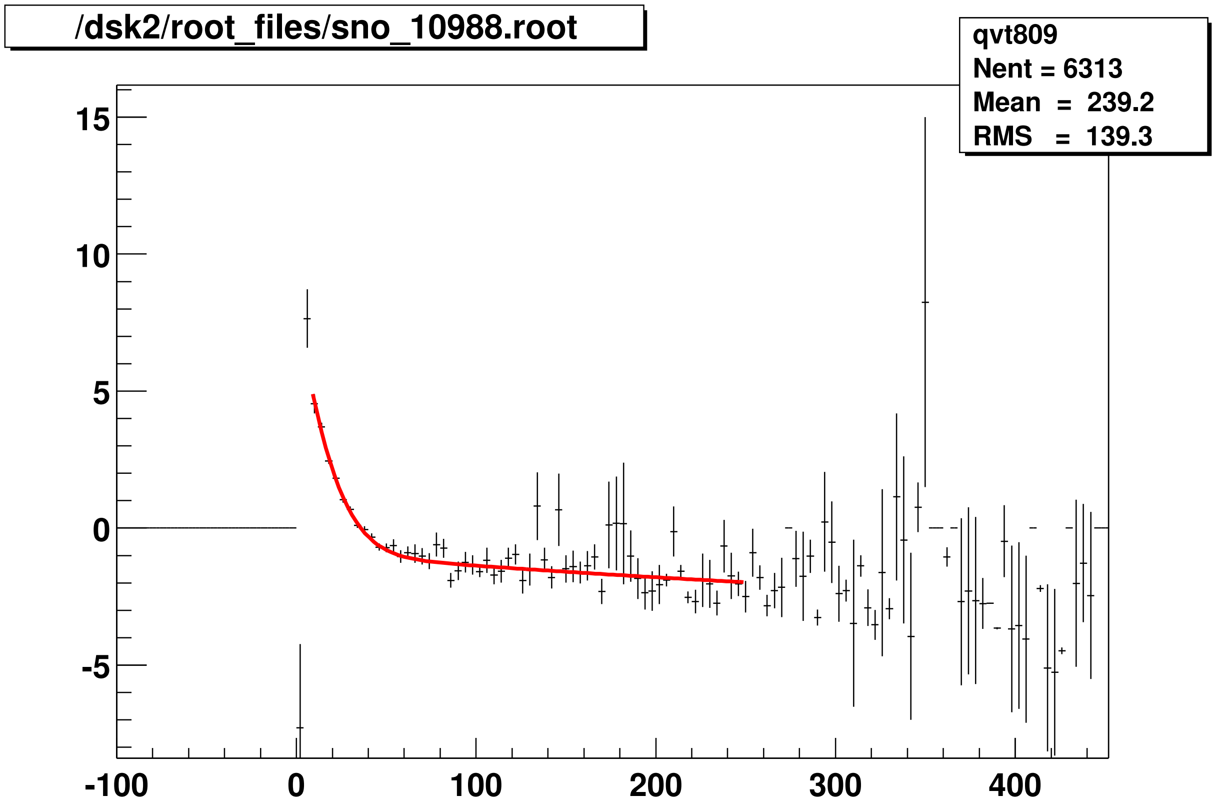

Figure 6: Figure 6. Q versus T for channel 1/9/9 . The solid line shows the fit to this channel.

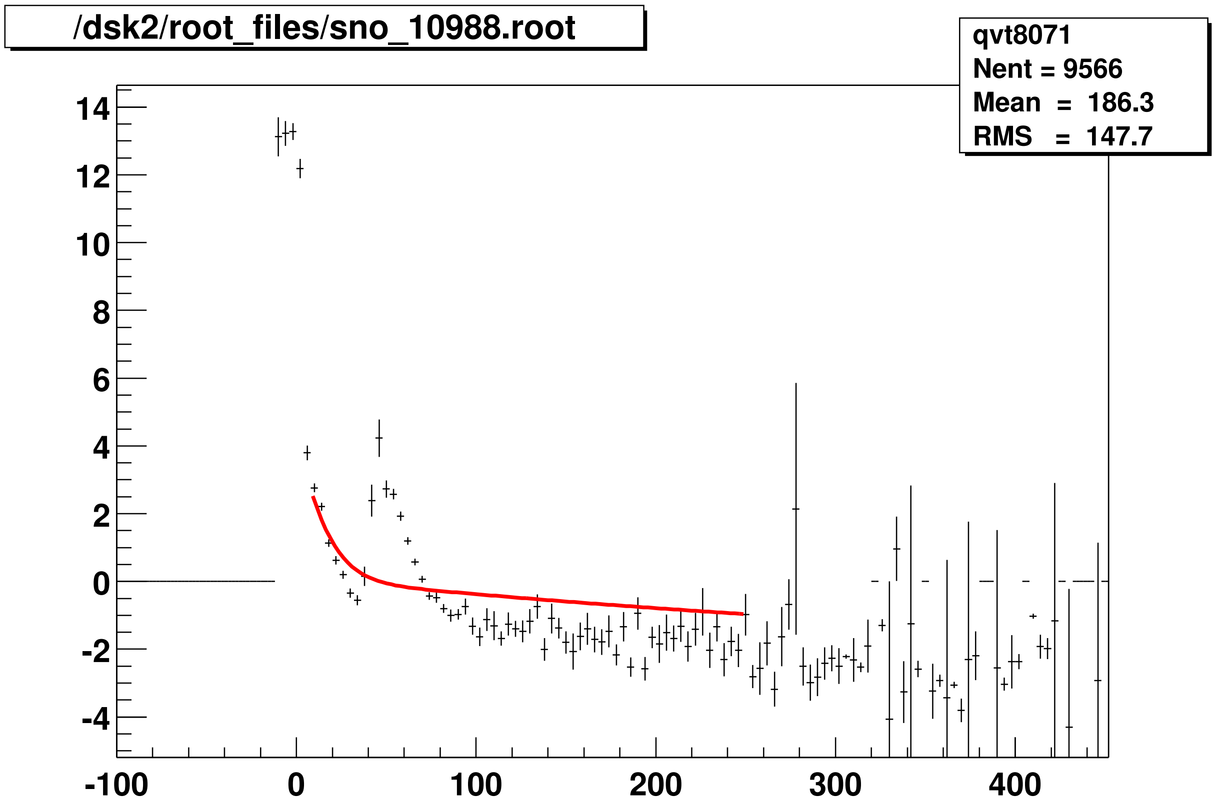

Figure 7: Figure 7. Q versus T for channel 15/12/7 .

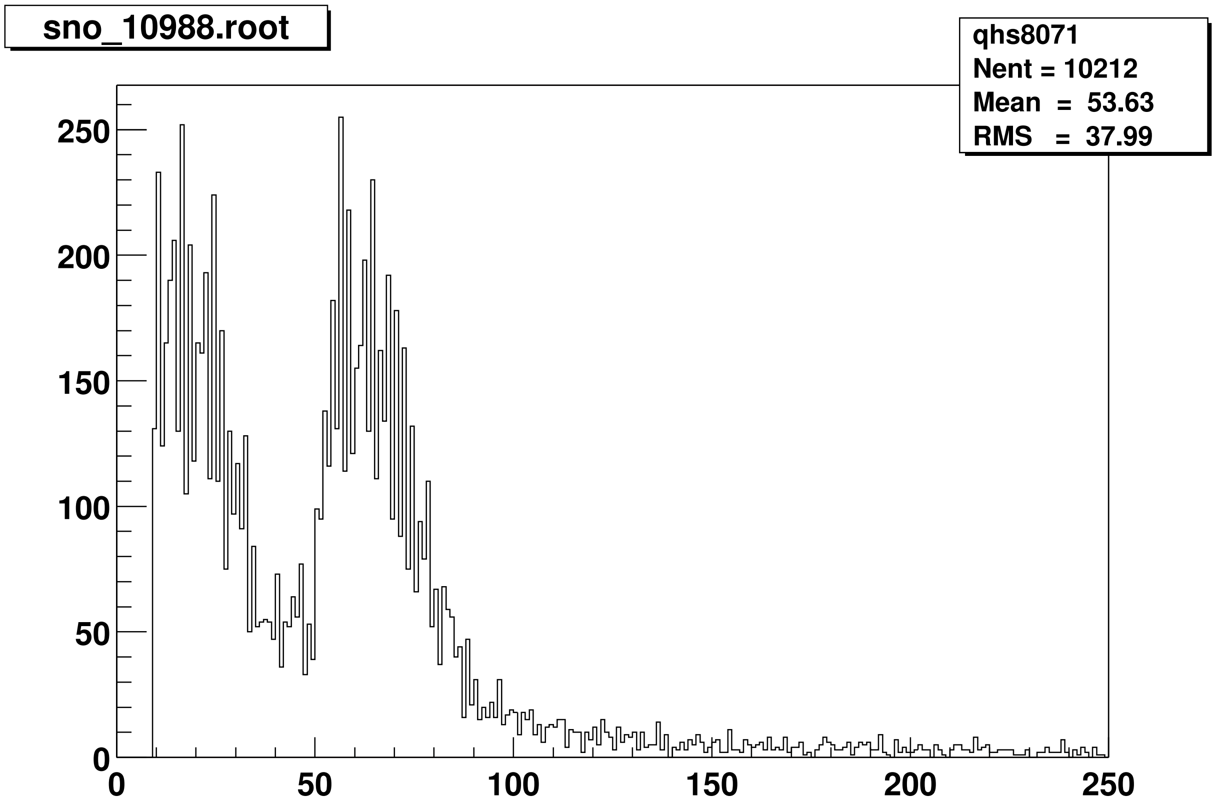

Figure 8: Figure 8. Q_{hs} for channel 15/12/7 .

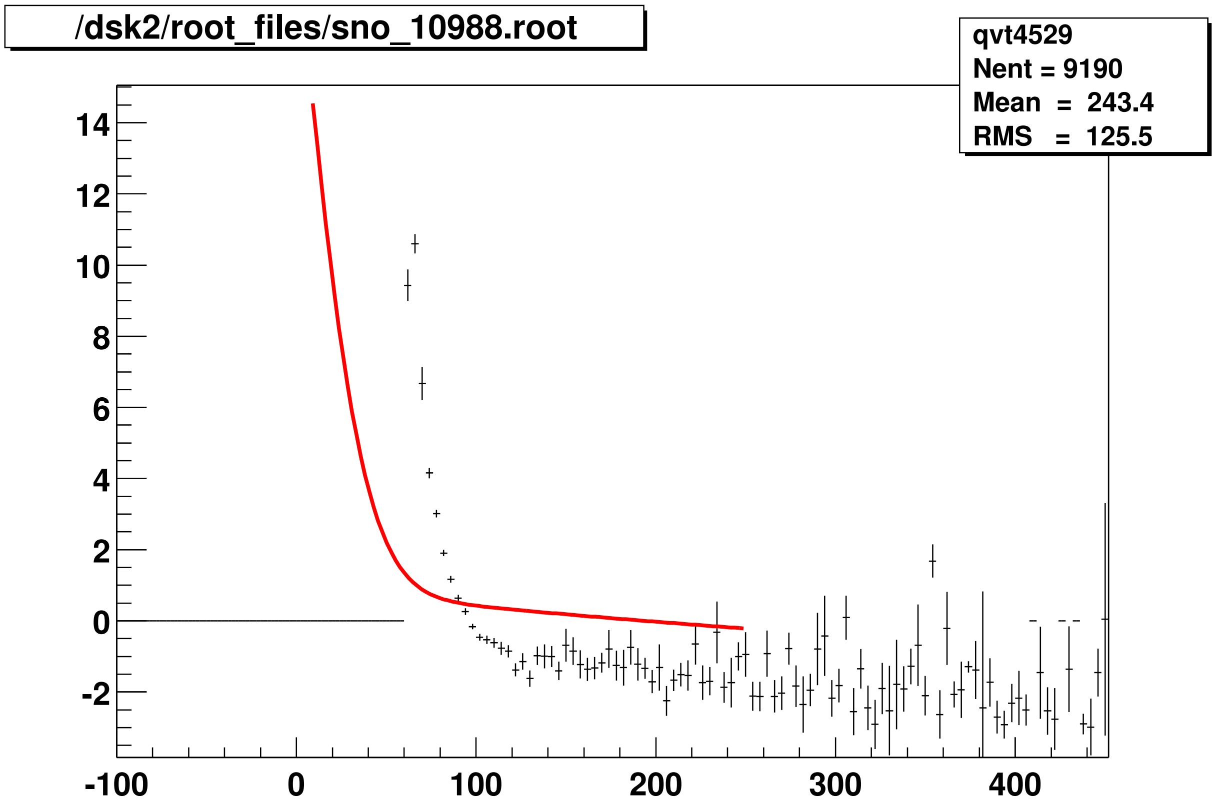

Figure 9: Figure 9. Q versus T for channel 8/13/17 .

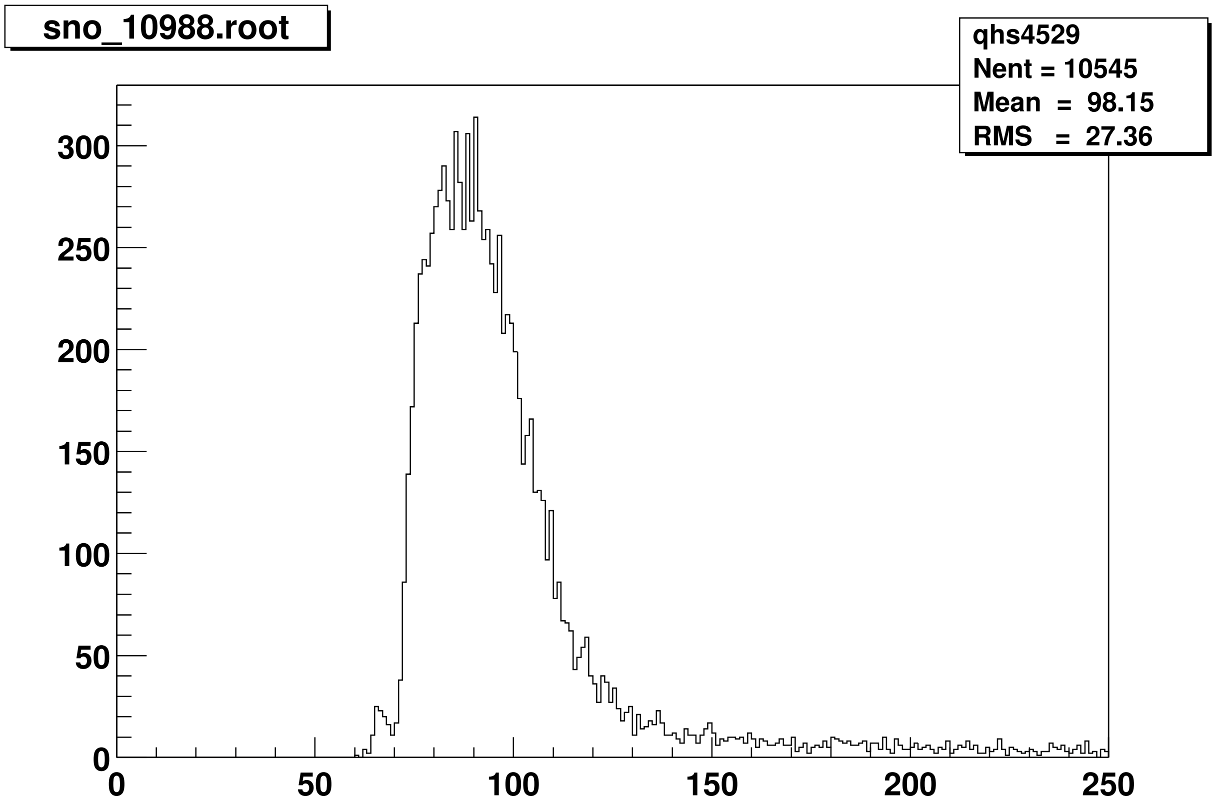

Figure 10: Figure 10. Q_{hs} for channel 8/13/17 . There is an obvious discrepancy between the ECA pedestal and the laser pedestal.

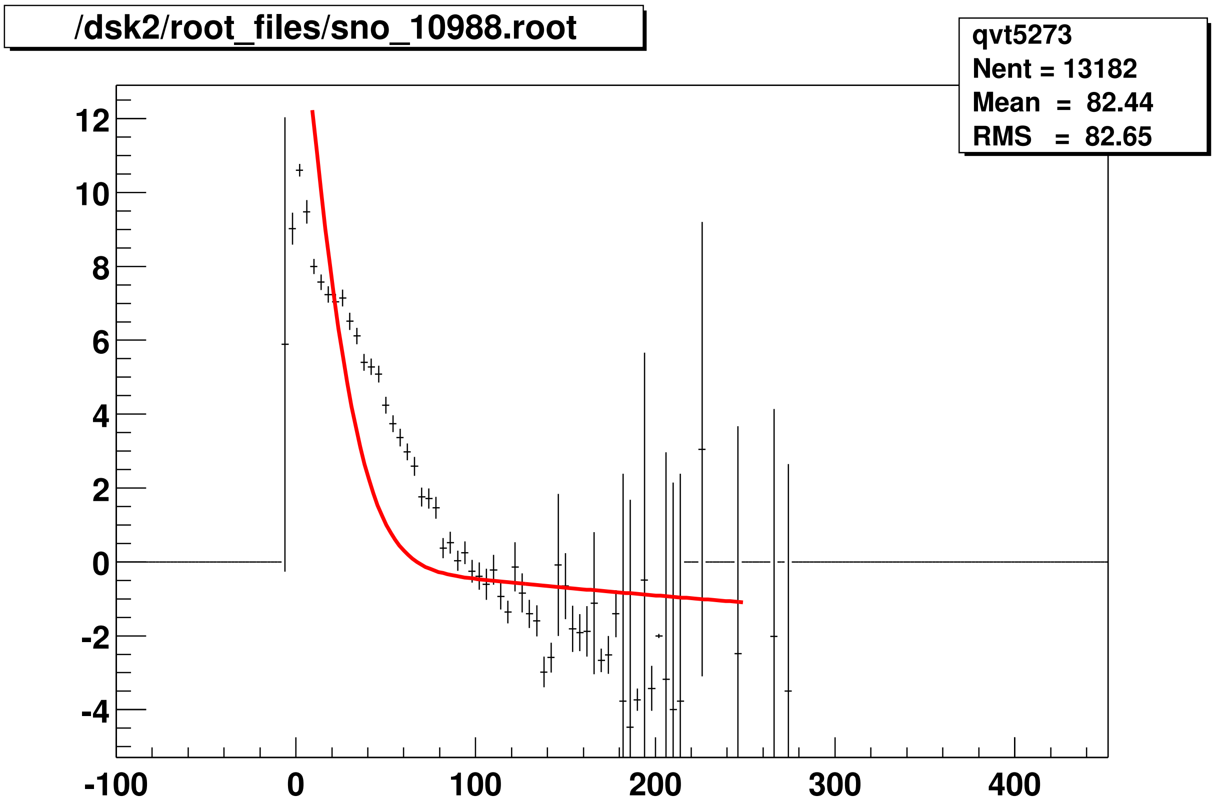

Figure 11: Figure 11. Q versus T for channel 10/4/25 .

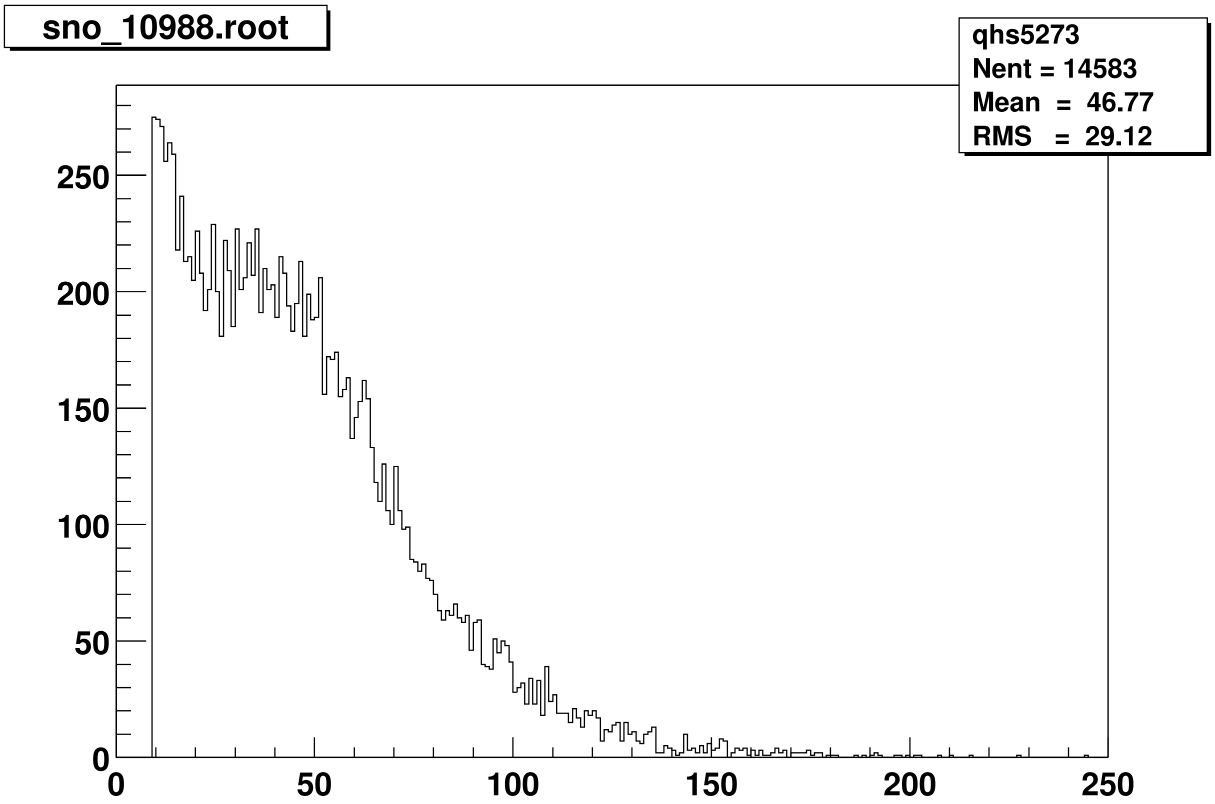

Figure 12: Figure 12. Q_{hs} for channel 10/4/25 .

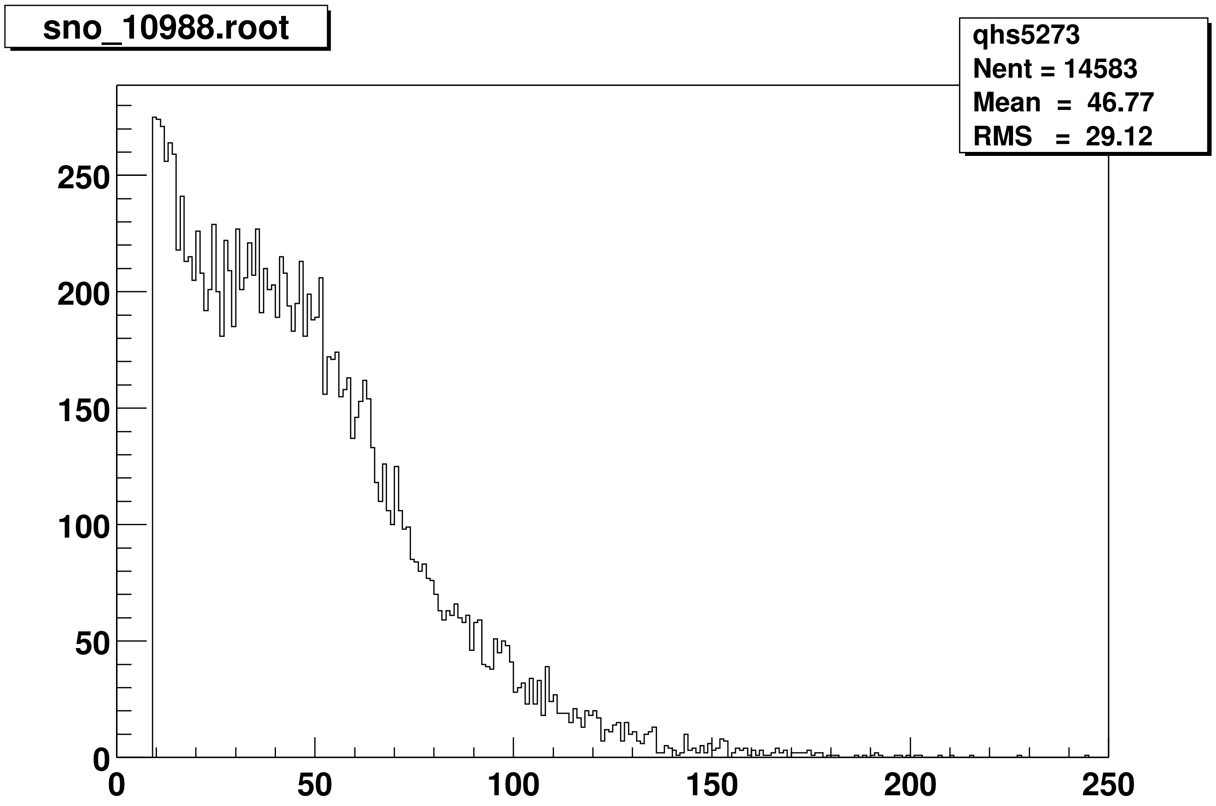

Figure 13: Figure 13. TAC histogram for channel 8/13/17 .

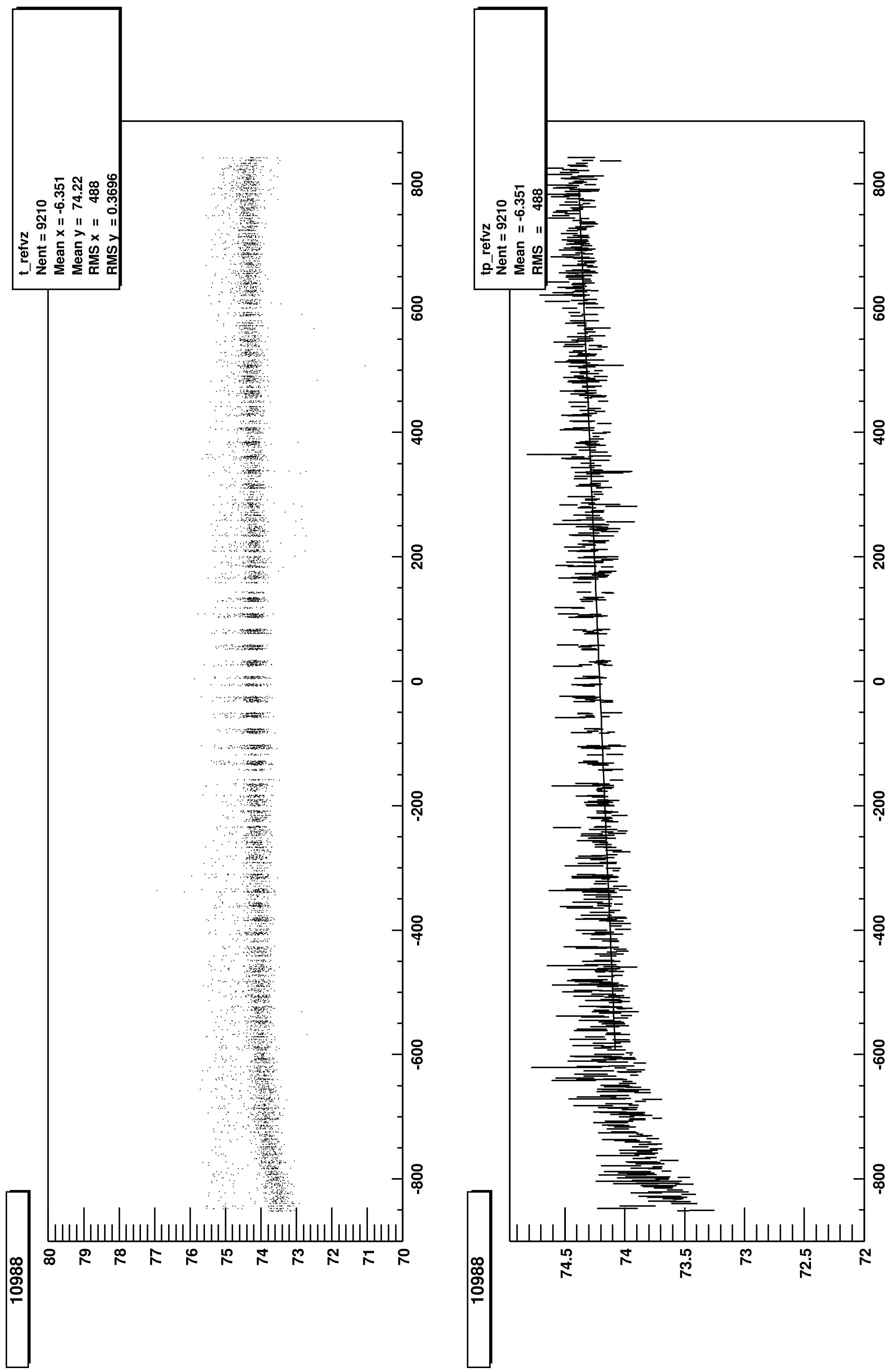

Figure 14: Figure 14. 180^0 degree reflection time as function of PMT z coordinate.

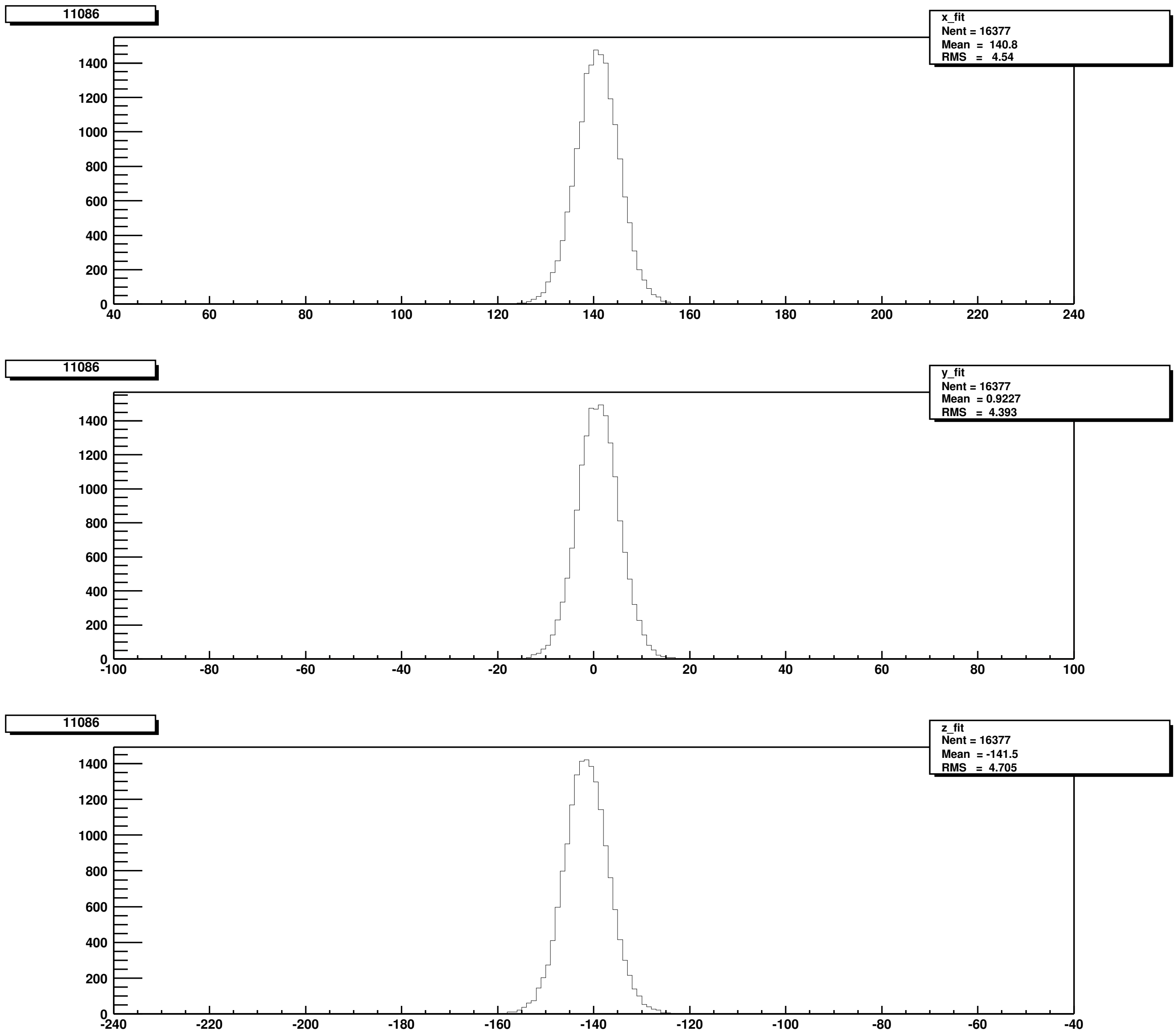

Figure 15: Figure 15. Reconstructed x, y and z distributions for run 11086 .

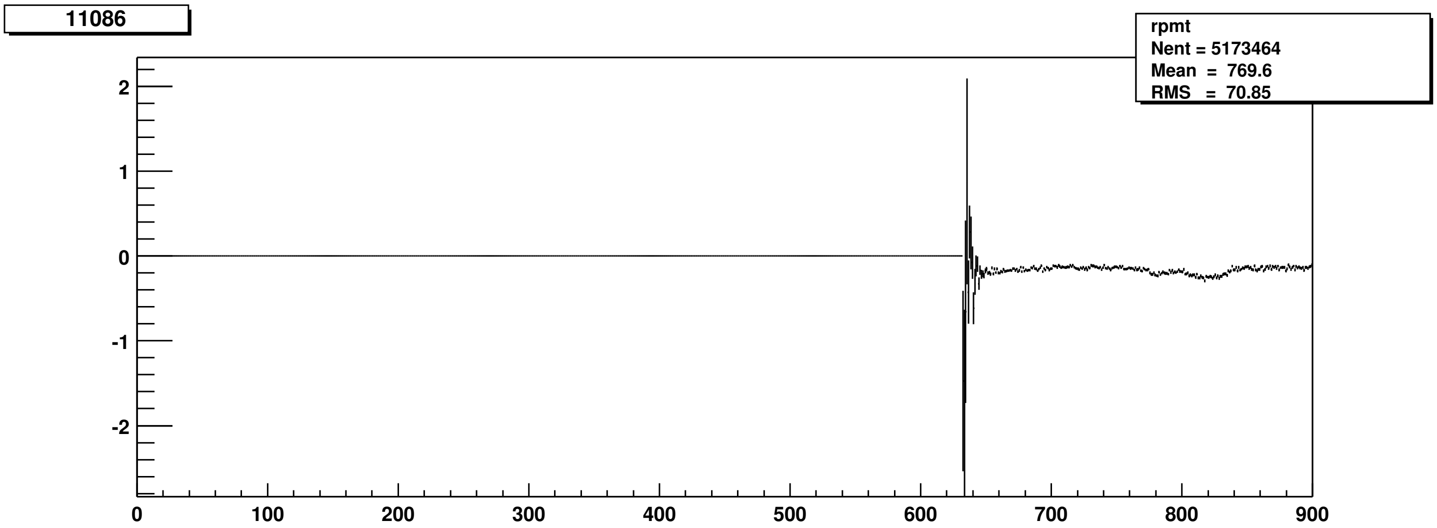

Figure 16: Figure 16. Distance to PMT versus time residual for run 11086 .

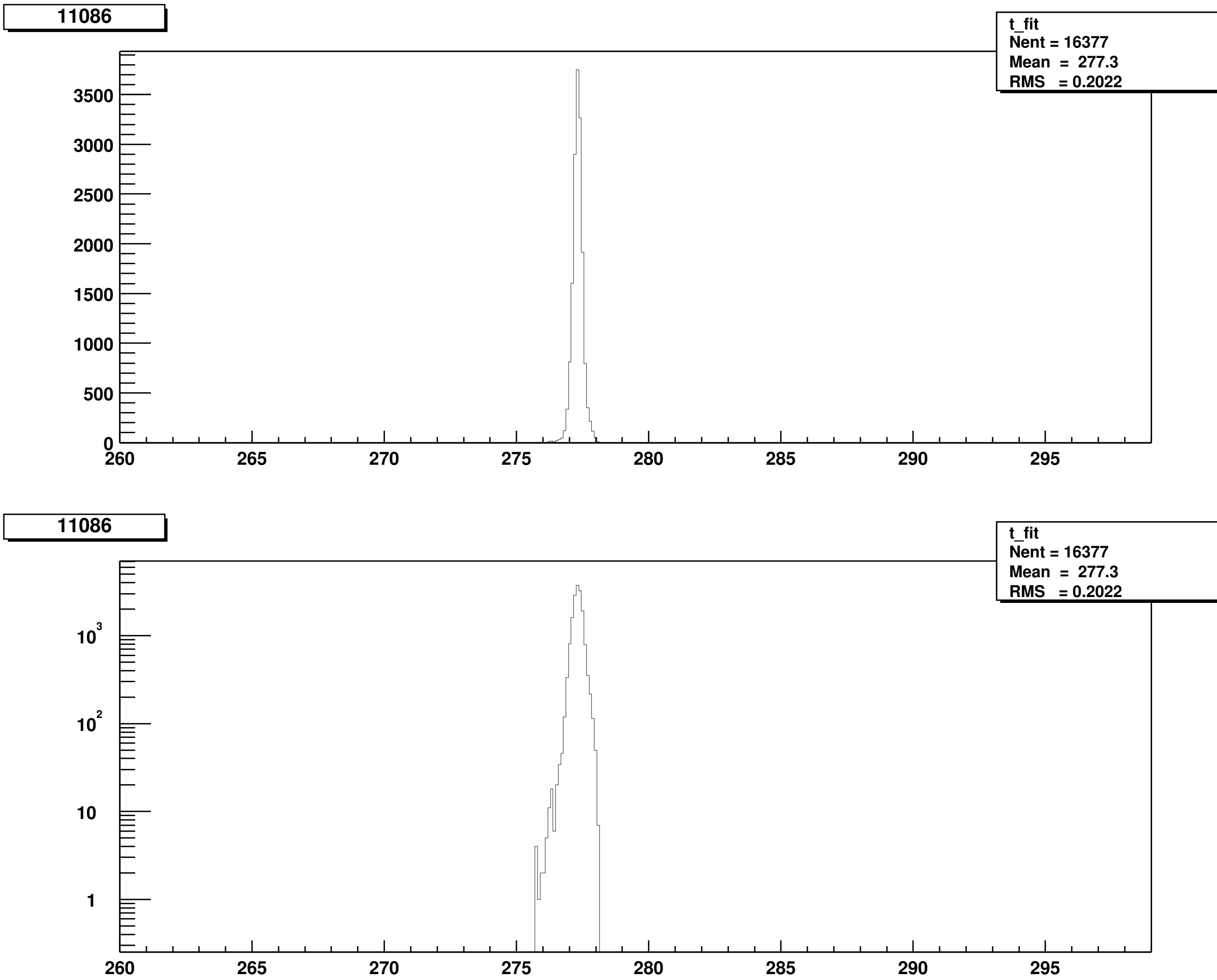

Figure 17: Figure 17. Reconstructed t for run 11086 .